The Aeronautical Journal (2024), **128**, pp. 1325–1343
doi:10.1017/aer.2024.54

ROYAL AERONAUTICAL SOCIETY

RESEARCH ARTICLE

Resolving nonuniform flow in gas turbines: challenges, progress, and moving forward

F. Lou

Institute for Aero Engine, Tsinghua University, Beijing, China
Email: loufy@tsinghua.edu.cn

Received: 10 October 2023; **Revised:** 24 April 2024; **Accepted:** 2 May 2024

Keywords: gas turbines; flow nonuniformity; Fourier-based approximation

Abstract

The flow in gas turbines exhibits a highly unsteady, complex and nonuniform manner, which presents two main challenges. Firstly, it introduces instrumentation errors, contributing to uncertainties when calculating one-dimensional performance metrics during rig or engine tests using fixed-location rakes. Secondly, it raises mechanical concerns, including high-cycle fatigue due to blade row interactions in turbomachines and thermal fatigue caused by hot-streaks at the combustor exit. Experimental characterisation of the flow nonuniformity in gas turbines is highly challenging due to the confined space and harsh environment for instrumentation. This paper presents recent efforts to address this issue by resolving the nonuniform flow in gas turbines using spatially under-sampled measurements. The proposed approach utilises discrete probe data and leverages a 'Fourier-based approximation' method developed by the author. The technique has undergone preliminary experimental validation involving reconstruction of the total pressure distribution in a multi-stage axial compressor and the total temperature field at the exit of the combustor and high-pressure turbine. Results show that, in the multi-stage axial compressor environment, reconstruction of inter-stage total pressure is achieved using a reduced dataset covering less than 20% of the annulus with reasonably good accuracy. The reconstructed total pressure yields almost identical mean total pressure values at all spanwise locations, with a maximum deviation of less than 0.02%. Additionally, reconstruction of the total temperature distribution at an engine-representative full annulus combustor is achieved using measurements at ten carefully selected circumferential locations. Results show that the reconstructed temperature field successfully captures the primary features associated with combustor exit temperature flow. The reconstructed temperature field yields excellent agreement in the magnitude of radial temperature distribution factor (*RTDF*) and overall temperature distribution factor (*OTDF*) predictions to the experiment, with a deviation of less than 0.5% for RTDF and less than 2.5% for OTDF. Lastly, reconstruction of the total temperature distribution at the exit of the GE E3 high-pressure turbine (*HPT*) is achieved using measurements at eight carefully selected circumferential locations. Results demonstrate remarkable robustness in resolving the temperature profile at the HPT exit with high fidelity, irrespective of the HPT inlet conditions. The initial validation results are promising, demonstrating that the new probe layout scheme and the Fourier-based approximation method enable effective characterisation of flow nonuniformity in gas turbines, thereby providing valuable insights into the complex flow of gas turbine engines.

Nomenclature

APU	auxiliary power unit
CFD	computational fluid dynamics
ESS	engine section stator
FOD	foreign object damage
HPT	high-pressure turbine

A version of this paper first appeared at the 26th Conference of the International Society for Air Breathing (ISABE), 22–27 September 2024, Toulouse, France.

IGV	inlet guide vane
OTDF	overall temperature distribution factor
RTDF	radial temperature distribution factor
S1	Stator No. 1
S2	Stator No. 2
URANS	unsteady Reynolds-averaged Navier-Stokes

Symbols

A	magnitude
$\boldsymbol{A}$	design matrix
$\boldsymbol{F}$	vector of unknown coefficients
h	enthalpy
k	condition number
N	number of wavelets
P	pressure
$\boldsymbol{W}_n$	wavenumber
$\boldsymbol{x}$	vector of measurements
$\boldsymbol{\theta}$	circumferential positions of the measurements
ρ	Pearson's coefficient

1.0 Introduction

The flow in gas turbines exhibits significant nonuniformity in both the radial and circumferential directions. There are three primary resources for the circumferential nonuniformities in gas turbines, including boundary conditions, geometric imperfections and blade row interactions, as shown in Fig. 1. Boundary conditions contribute to circumferential nonuniformities through inlet distortions and downstream potentials. Geometric imperfections arise from manufacturing inconsistencies, eccentricities, foreign object damage (FOD), erosion and wear, among other factors. Blade row interactions play a crucial role in introducing nonuniformities for flow in turbomachines, involving wakes from upstream stator row(s), potential fields from upstream and downstream stator rows and their aerodynamic interactions.

The impacts of circumferential flow nonuniformity are twofold. Firstly, it can introduce instrumentation errors, exacerbating uncertainties when calculating one-dimensional performance metrics during rig or engine tests utilising fixed-location rakes. Secondly, it gives rise to mechanical concerns, including high-cycle fatigue resulting from blade row interactions in turbomachines and thermal fatigue due to hot-streaks at the combustor exit.

1.1 Nonuniform flow everywhere in gas turbines

Nonuniform flow is prevalent in various components, including engine intakes, compressors, turbines and others. Nevertheless, it is important to note that the primary mechanism and dominant flow features of the nonuniformity can differ significantly in each component, as illustrated in Fig. 2. A comprehensive analysis of these variations will be conducted in the subsequent sections to gain a deeper understanding of the distinct characteristics associated with each component.

1.1.1 Nonuniform flow in intakes

There are three representative intakes for gas turbines, including the pitot-type inlet, S-duct inlet and auxiliary power unit (APU) style inlet. These intake designs cater to specific applications. Civil aircraft typically employ high-bypass-ratio turbofan engines with pitot-type intakes, modern military aircrafts such as air-superiority fighters commonly utilise S-duct inlets, and APU-style inlets are widely used in auxiliary power units or gas turbines for land- and sea-based applications. Sketch of these intakes and the corresponding flow patterns are shown in Fig. 3. A well-designed pitot-type inlet delivers distortion-free flow into the aero engine [1]. However, in the case of S-duct inlets or APU-style inlets, curvature

https://doi.org/10.1017/aer.2024.54 Published online by Cambridge University Press

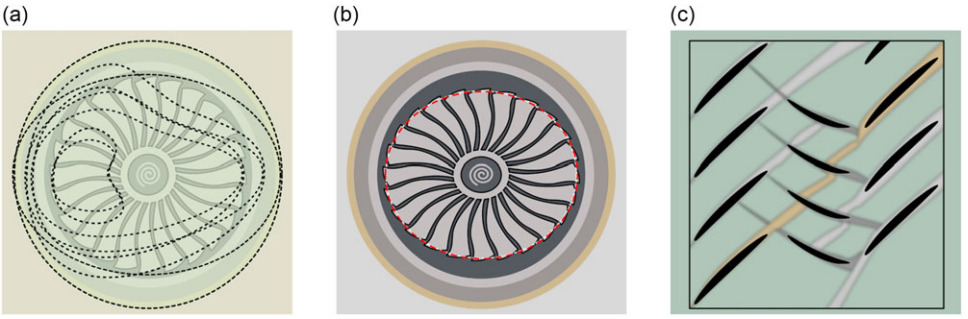

Figure 1. *Resources for circumferential nonuniformities in gas turbines including: (a) boundary conditions, (b) geometric imperfections, and (c) blade row interactions.*

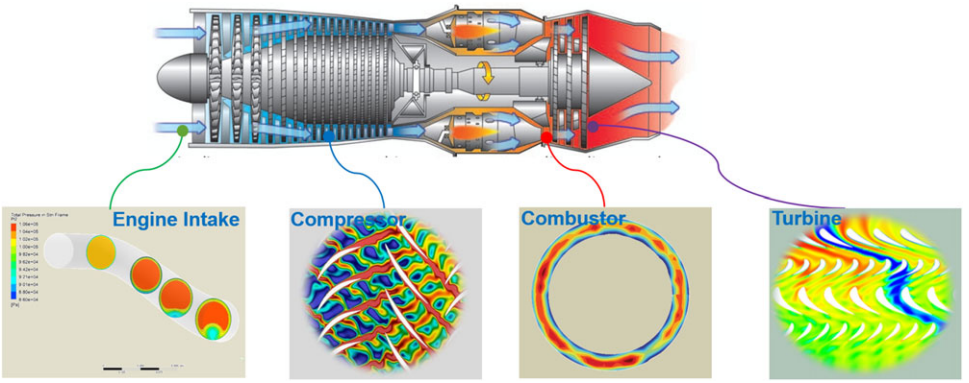

Figure 2. *Illustrations of nonuniform flow patterns in gas turbines.*

effects come into play, introducing swirl distortion downstream of the engine, as illustrated in Fig. 3(b) and (c). These swirling flows result in various patterns, including bulk swirl, twin swirl or offset swirls [2, 3]. Understanding and managing these flow patterns are crucial in optimising the performance of gas turbine systems.

1.1.2 Nonuniform flow in compressors

The flow field in a compressor is nonuniform in both radial and circumferential directions. Radial nonuniformity arises due to the development of boundary layers along the hub and shroud surfaces. On the other hand, circumferential nonuniformities are associated with the wakes from upstream stator row(s), potential fields from both upstream and downstream stator rows, and their aerodynamic interactions, as shown in Fig. 4(a). Research shows that specific wavenumbers typically dominate the circumferential flow in multi-stage compressors. For instance, the study conducted by Chilla et al. [4] on the circumferential variations of the stagnation pressure and temperature flow field in an eight-stage axial compressor representative of an aero-engine core compressor found that the dominant wavenumber in the front and middle of the compressor corresponds to the upstream stator vane count. In contrast, the rear of the compressor is influenced by the wavenumber associated with the struts in the exit duct. Figure 4(a) depicts the circumferential total pressure field and the corresponding dominant wavenumbers at the compressor's mid-span upstream of Stator 6 [4]. The circumferential total pressure field variations are primarily governed by seven wavenumbers associated with the vane counts of the blade rows upstream and downstream of Stator 6 (ranging from ESS/IGV to S6).

https://doi.org/10.1017/aer.2024.54 Published online by Cambridge University Press

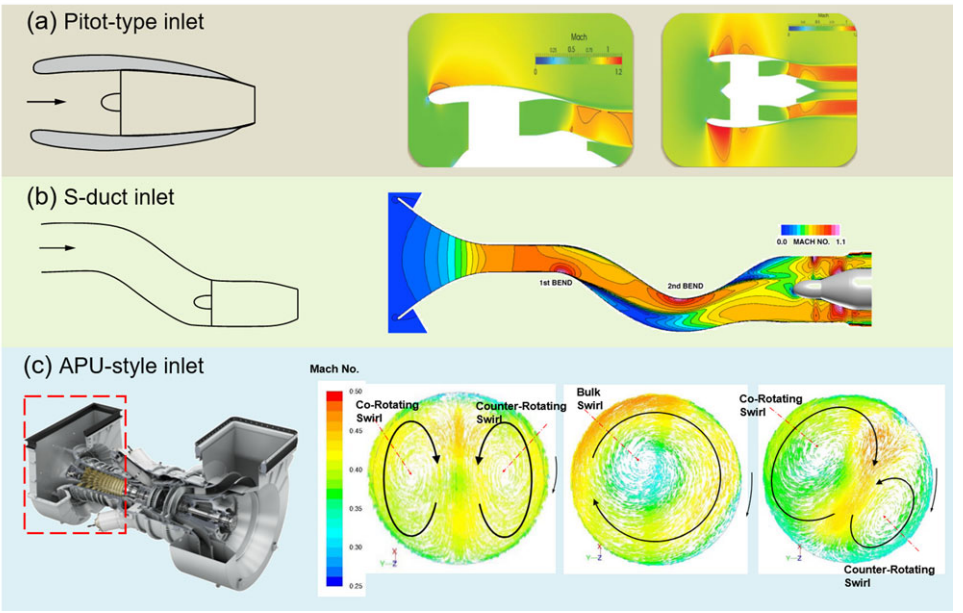

Figure 3. *Representative gas turbine intakes and the corresponding flow patterns: (a) pitot-type inlet, (b) S-duct inlet, and (c) APU-style inlet. Adapted from Refs [1–3].*

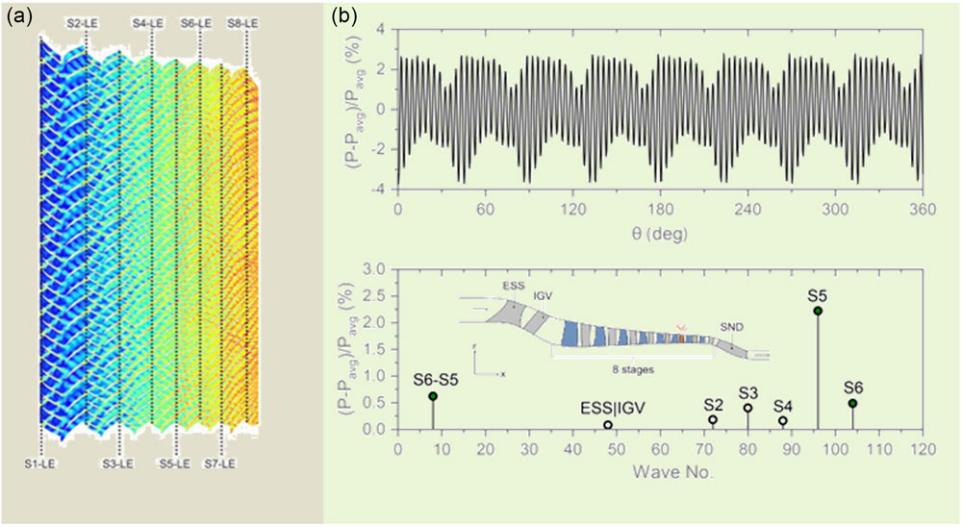

Figure 4. *Total pressure distribution in an eight-stage axial compressor at mid-span (a) contour of total pressure and (b) non-dimensional total pressure downstream of Stator 6, adapted from Ref. [4].*

Figure 5 shows the normalised total pressure field downstream of the first two stators in a three-stage axial compressor, covering half of the annulus [5]. This experiment was conducted in the Purdue 3-Stage (P3S) Axial Compressor Research Facility, utilising the PAX100 compressor with a reduced vane count for Stator 1, referred to as PAX101 [6]. The total pressure is normalised by the area-averaged total pressure at the compressor inlet, and the solid symbols indicate the spanwise probe locations. Significant passage-to-passage variations are evident in the total pressure field downstream of Stator 1

https://doi.org/10.1017/aer.2024.54 Published online by Cambridge University Press

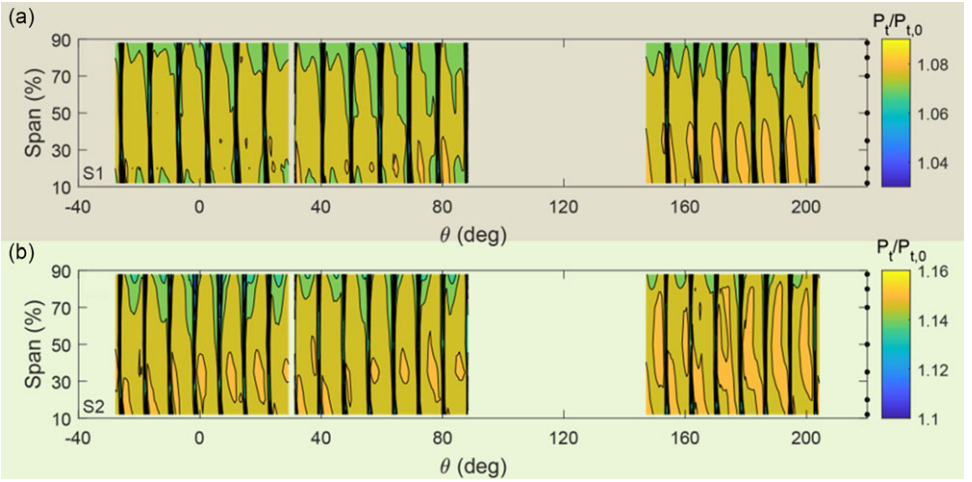

Figure 5. *Normalised total pressure contours downstream of (a) the first stage and (b) the second stage, adapted from Ref. [5].*

(S1) and Stator 2 (S2). Additionally, a repetitive pattern emerges concerning the size and shape of the low-momentum flow along the suction surface near the shroud, cyclically occurring approximately every 60 degrees. While various factors contribute to the observed passage-to-passage variations, including geometric imperfections, the primary driver behind these fluctuations lies in the interactions between blade rows. Notably, wake-wake interactions and wake-potential field interactions play a dominant role in shaping the flow patterns. The most important wavenumbers can be determined according to the following guidelines:

- Wake effects: Consider the upstream vane counts or upstream struts
- Potential effects: Take into account the upstream and downstream vane counts or upstream and downstream struts
- Clocking effects: Examine the differences between the upstream and downstream vane counts

1.1.3 Nonuniform flow in combustors

The temperature field at the combustor exit exhibits a highly three-dimensional nature, characterised by substantial radial and circumferential variations. These circumferential temperature fluctuations, commonly referred to as 'hot-streaks', arise due to the discrete nature of fuel and dilution air jets, while the presence of combustor lining coolant flow results in a pronounced radial temperature gradient. For instance, Fig. 6(a) illustrates a whole-field combustor exit temperature profile obtained at the exit plane of a typical can-annular combustor featuring 20 fuel injectors in a military engine [7]. The measured nondimensional temperature ranged from 0.59 to 1.24 with a mean temperature of 2,072K. Significant nonuniformities are evident along the radial direction, with relatively low-temperature regions observed at the hub and casing end walls due to the influence of the combustor liner coolant flow. Furthermore, the circumferential variations (hot-streaks) are also prominent, exhibiting distinct burner pitch-to-pitch variations. These complex and varying temperature patterns are crucial factors to consider when analysing the performance and efficiency of combustors in gas turbine engines.

Two parameters commonly used to quantify combustor exit temperature nonuniformity are the radial temperature distribution factor (RTDF) and the overall temperature distribution factor (OTDF).

https://doi.org/10.1017/aer.2024.54 Published online by Cambridge University Press

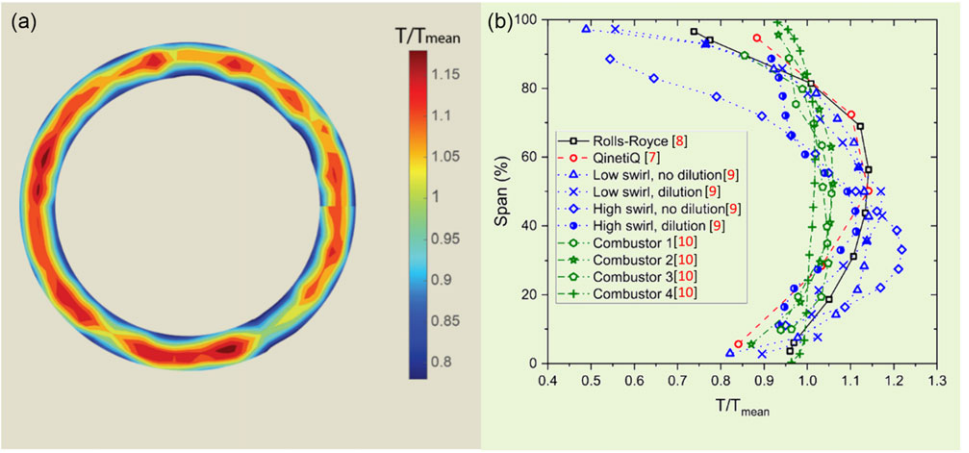

Figure 6. *Nonuniform total temperature field at combustor exit: (a) Nondimensional total temperature contour [7] and (b) summary of engine representative combustor exit radial temperature profiles, adapted from Ref. [11].*

The RTDF serves as a profile factor, assessing the nonuniformity of the circumferentially averaged temperature field. On the other hand, the OTDF acts as a pattern factor, gauging the deviation of the hottest gas streak from the mean temperature. Their definitions are as follows:

$$RTDF = \frac{\bar{T}^{cir}_{4,\max} - \bar{T}^{area}_{4}}{\bar{T}^{area}_{4} - \bar{T}^{area}_{3}} \tag{1}$$

$$OTDF = \frac{T_{4,\max} - \bar{T}^{area}_{4}}{\bar{T}^{area}_{4} - \bar{T}^{area}_{3}} \tag{2}$$

On one hand, the total temperature profiles at the combustor exit are heavily influenced by the burner design and operating conditions, such as whether it operates under rich burn or lean burn conditions. On the other hand, only very few examples of whole-field temperature measurements are published in the open literature, primarily due to the sensitive and confidential nature of such data and the high costs associated with conducting such experiments. Consequently, there is a lack of consensus regarding the magnitude or intensity of hot streaks at the combustor exit in gas turbine engines. As an illustration, Fig. 6(b) compiles the nondimensional combustor exit radial temperature profiles from datasets available in the open literature, encompassing four different combustor geometries and ten experimental datasets [7–10]. These limited data points underline the challenges in obtaining comprehensive and representative information on combustor exit temperature patterns in the public domain.

Despite the scarcity of data in the open literature, research showed that combustor exit temperature profiles exhibiting pronounced hot-streaks and demonstrating excellent burner pitch-to-pitch symmetry tend to exhibit a dominant single wavenumber in the total temperature circumferential nonuniformity. This wavenumber value corresponds to the number of fuel injectors present [11]. However, in practical applications, the existence of burner pitch-to-pitch variations introduces additional components in the spatial-frequency domain, complicating the temperature patterns and resulting in a more diverse range of wavenumbers being present.

1.1.4 Nonuniform flow in turbines

Given the considerable nonuniform temperature field at the HPT inlet, the circumferential nonuniformities within a high-pressure turbine are a result of a combination of factors, namely, the migration of inlet

https://doi.org/10.1017/aer.2024.54 Published online by Cambridge University Press

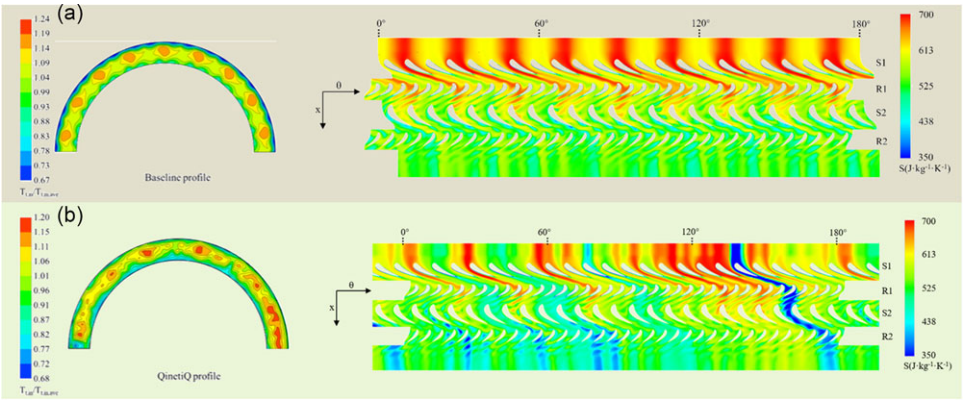

Figure 7. *Nonuniform total temperature field across a two-stage high-pressure turbine: (a) baseline case with symmetric inlet hot-streaks and (b) case with engine representative inlet hot-streaks with significant asymmetry, adapted from Ref. [12].*

hot-streaks and interactions with the turbine blade rows. Figure 7 provides insight into the migration of hot-streaks across the GE E3 two-stage HPT at mid-span [12]. Two cases were examined: the baseline case featuring perfectly periodic hot-streaks and the QinetiQ case [7] with aperiodic hot-streaks at the HPT inlet. Snapshots of the instantaneous entropy at mid-span were captured for both cases and are depicted in Fig. 7(a) and (b), respectively. In the baseline case, a repetitive pattern of alternating entropy was observed at the HPT inlet, aligning with the periodic inlet temperature distribution. Conversely, in the QinetiQ case [7], the entropy distribution at the HPT inlet exhibited less periodicity attributed to the variations between burners. As the hot-streaks migrate across the HPT blade rows, both cases experienced a more intricate entropy pattern primarily due to blade row interactions. Hot-streaks remained evident at the HPT exit for both cases, consistent with findings reported in Refs [13, 14]), which emphasises the persistence and influence of hot-streaks on the flow field throughout the high-pressure turbine stages.

To illustrate the evolution of the driving mechanism for circumferential temperature nonuniformity across the HPT, Fig. 8 presents the migration of hot-streaks in terms of time-averaged total temperature and corresponding spatial fast Fourier transform (SFFT) results for both the baseline case with perfectly periodic hot-streaks (Fig. 8(a)) and the QinetiQ case [7] featuring aperiodic hot-streaks at the HPT inlet. In the baseline case, as expected, hot-streaks predominantly contribute to the circumferential temperature nonuniformity at the HPT inlet. However, at the HPT exit, additional factors come into play, including the wakes of the upstream stators, interactions of the upstream stators and interactions of hot-streaks with the second stator. In general, the presence of burner-to-burner asymmetry does not alter the overall trend of hot-streak migration. For instance, the magnitude of hot-streaks undergoes more attenuation across rotors than across vane rows or stators. Despite the rapid decay of hot-streaks from the HPT inlet to exit, their impact on the temperature distribution at the HPT exit remains significant for both cases. Nevertheless, the burner-to-burner asymmetry results in a more scattered energy distribution across the spatial domain, as shown in Fig. 8(b).

Hence, in turbines, the dominant wavenumbers can be identified using the following guidelines:

- Effects of inlet hot-streaks: Consider the number of distinct hot-spots present at the inlet.
- Wake effects: Examine the upstream vane counts or the presence of upstream struts.
- Potential effects: Take into account the upstream and downstream vane counts or upstream and downstream struts.
- Clocking effects: Analyse the differences between the upstream and downstream vane counts.

https://doi.org/10.1017/aer.2024.54 Published online by Cambridge University Press

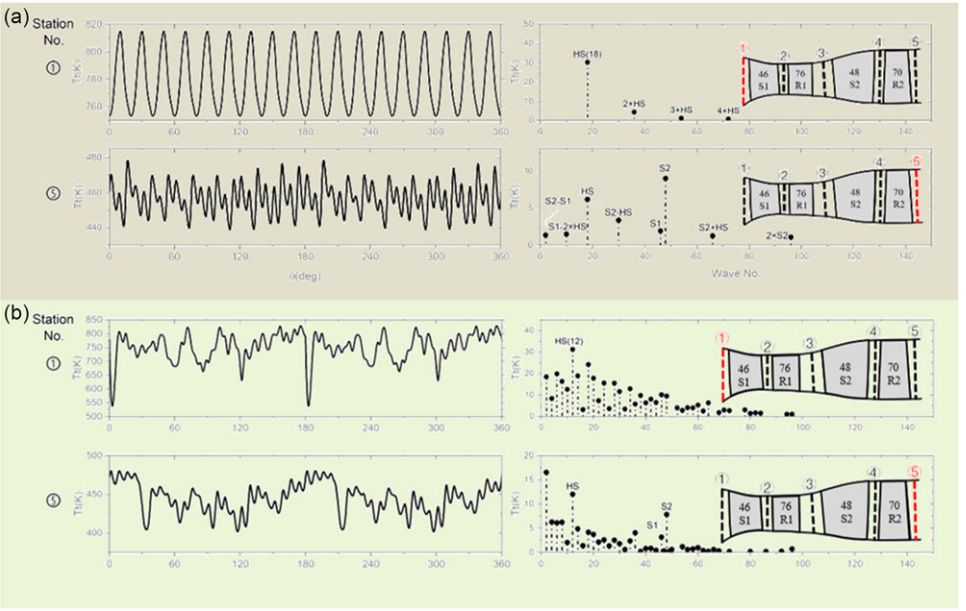

Figure 8. *Nonuniform total temperature profile at HPT inlet and exit: (a) baseline case with symmetric inlet hot-streaks and (b) case with engine representative inlet hot-streaks with significant asymmetry, adapted from Ref. [12].*

1.2 Influence of the nonuniform flow

The influences of circumferential flow nonuniformity are twofold. Firstly, it can lead to instrumentation errors, adding to the uncertainties when calculating one-dimensional performance metrics during rig or engine tests using fixed-location rakes. Secondly, it raises mechanical concerns, such as high cycle fatigue resulting from blade row interactions in turbomachines or thermal fatigue due to hot-streaks at the combustor exit. For instance, the pressure circumferential nonuniformities in turbomachines create challenges in characterising the aerodynamic blade forcing function for forced response because of the passage-passage variations caused by blade row interactions, essentially contributing an aerodynamic mistuning to the wake forcing function; while the circumferential temperature nonuniformity from the exit of the combustor can cause the failure of NGVs.

1.2.1 Aerothermal performance

In engine or rig tests, one-dimensional performance metrics are determined based on measurements obtained from rakes positioned at fixed axial locations around the annulus [15]. These measurements are then averaged to derive a representative mean flow property [16]. However, when dealing with blade rows featuring dissimilar vane counts leading to 'aperiodic' flow among passages around the annulus, the data acquired at discrete locations can become biased and contribute to uncertainties, commonly referred to as instrumentation errors, in the reduced one-dimensional performance metrics. For example, Stummann et al. [17] conducted a full-annulus URANS simulation in a 3.5-stage axial compressor at midspan and demonstrated that the circumferentially non-uniform flow can result in more than a one-point error in compressor stage performance measurements. More recently, Methel et al. [18] experimentally characterised the stator wake variability in a three-stage axial compressor through a comprehensive traverse of different vane passages. The results revealed variations of up to three points in overall compressor efficiency and up to 15 points in individual stage efficiency-based on pressure and temperature variations observed among passages. Similar conclusions were drawn for turbine performance evaluations,

https://doi.org/10.1017/aer.2024.54 Published online by Cambridge University Press

although they are not discussed in detail here. As designers now make design choices that lead to efficiency improvements on the order of 0.1 points, the uncertainty introduced by instrumentation errors presents a challenge in accurately assessing the magnitude of performance improvements in technology development programs.

1.2.2 Mechanical concerns

In addition to the concern about the failure of NGVs due to the circumferential temperature nonuniformities at the combustor exit, high-cycle fatigue of rotors in gas turbines resulting from flow-induced resonant vibratory responses has been a long-standing priority for the gas turbine community. However, while considerable progress has been made in predicting mistuned forced responses [19, 20], the understanding of the influence of circumferential flow nonuniformity on aerodynamic excitation remains limited. The primary causes of excitation are considered to be the wake from the upstream blade row and the potential field from the downstream blade row. Typically, the aerodynamic excitation derived from steady single-passage CFD simulations is used to predict the rotor's resonant response. Nevertheless, Schoenenborn [21] demonstrated that the aerodynamic excitation can vary significantly from blade to blade due to the superposition of the Tyler-Sofrin (or scattered or spinning) modes. Moreover, recent research by Methel et al. revealed more than 60% variations in spectral magnitudes of the fundamental forcing frequency due to stator wake variability among the investigated passages [18]. Therefore, accurate prediction of aerodynamic blade forcing functions is gaining importance as it drives rotor resonant vibratory response.

1.3 Challenges in characterising the nonuniform flow

In most scenarios, characterising nonuniform flow in engine-level tests is unfeasible due to limited instrumentation capacity or adverse environment. As a result, component-level rig tests are employed to facilitate detailed flow investigations. In the case of combustor rig tests, the state-of-the-art approach to account for the impact of combustor exit temperature nonuniformities, considering both profile and pattern factors, involves conducting an extensive traverse test campaign. This process requires a complex traverse mechanism. For instance, the current standard practice involves making measurements at intervals as fine as one measurement per every 1.5° to 3° (equivalent to 240–120 traverses) to effectively characterise the entire field at the combustor exit plane.

In rig tests of turbomachines, such as compressors and turbines, characterising circumferential variations in the flow field can be accomplished through circumferential traverses across single or multiple flow passages, either utilising a probe traverse mechanism or fixed instrumentation while actuating the stator rows circumferentially. However, this involves costly design and development of complex traverse mechanisms and introduces challenges in sealing the flow path. An alternative approach is placing probes behind different blades at different relative pitchwise positions to capture the free and wake flow separately. By integrating all these measurements, a representative single-passage profile is derived, assuming periodic flow from passage to passage, as depicted in Fig. 9(a). This concept of passage-to-passage periodicity is also commonly used in single-passage numerical simulations, as illustrated in Fig. 9(b). However, as discussed in the previous section, in a multi-stage environment with dissimilar vane counts for blade rows, there is evident flow variability leading to 'aperiodic' flow among passages around the annulus. In such cases, all the approaches based on the assumption of periodic flow from passage to passage may produce skewed passage profiles and mean values, which can impact the accuracy and reliability of the results obtained from rig tests or single-passage numerical simulations.

2.0 Recent progress

Can the complex and highly nonuniform flow in gas turbines be adequately resolved with spatially undersampled measurements? Addressing this question, a novel concept known as the 'flow approximation

https://doi.org/10.1017/aer.2024.54 Published online by Cambridge University Press

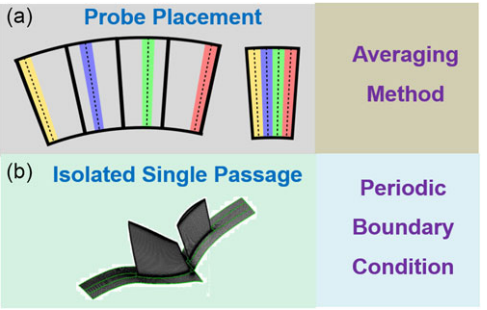

Figure 9. *Sketch of the state-of-the-art experimental and numerical approaches.*

method' has emerged recently. This idea revolves around identifying and characterising dominant flow features using discrete measurements. Several groups of researchers have made notable progress in approximating the flow field in turbomachines through such approaches. For instance, Chilla et al. [4, 22] explored the estimation of compressor flow using a single harmonic. Seshadri et al. devised a technique to reconstruct the 2D temperature spatial field employing a multivariate linear least-squares model with Tikhonov regularisation, while also considering uncertainty assessment [23, 24]. More recently, Seshadri et al. [25] introduced a transfer learning model suitable for temperature and pressure approximation in aero engines based on the similarity of measurements at different planes. Cruz et al. [26] presented a novel data assimilation technique that couples numerical modelling and experimental data using Bayesian inference, successfully applying it to a small aspect ratio axial compressor. The flow field reconstruction was achieved even with a 70% random under-sampling of complete measurements [27].

Meanwhile, Lou and Key devised a systematic framework for reconstructing circumferential non-uniform flow utilising a 'multi-wavelet approximation' method [28]. Subsequently, this method was successfully applied to various experiments involving measurements in compressors [29], combustors [11], and a high-pressure turbine [12], yielding quite promising results. The method is indeed a Fourier-based approximation approach, and irrelevant to wavelet transformation. As a result, in the present study, the terminology 'Fourier-based approximation' is adopted to eliminate possible confusion with wavelet theory. As a result, this section will primarily concentrate on the author's previous work, providing an overview of the methodology and its applications in these contexts.

2.1 Fourier-based approximation method

In theory, the circumferential flow field in gas turbines with a spatial periodicity of 2π can be described in terms of infinite serial of *sine* and *cosine* functions:

$$x(\theta) = c_0 + \sum_{i=1}^{\infty} \left(\mathrm{a}_i \sin\left(W_{n,i}\theta\right) + \mathrm{b}_i \cos\left(W_{n,i}\theta\right)\right) \tag{3}$$

in which, $x(\theta)$ represents the flow property along the circumferential direction, c_0 represents the DC component of the signal.

Research shows that the circumferential flow in gas turbines is typically dominated by several Fourier series. Thus, it is possible to approximate the circumferential variations of the flow field in gas turbines using a few (N) dominant Fourier series instead of an infinite number of Fourier series:

$$x(\theta) \approx c_0 + \sum_{i=1}^{N} \left(a_i \sin\left(W_{n,i}\theta\right) + b_i \cos\left(W_{n,i}\theta\right)\right) \tag{4}$$

To solve for the information for the N dominant wavelets in Equation (4), a minimum of $2N+1$ data points measured at different circumferential locations, $\boldsymbol{\theta} = (\theta_1, \theta_2, \theta_3, \cdots, \theta_m)$, is required. This is an important step toward reconstructing the circumferential flow field since it reduces the number of

https://doi.org/10.1017/aer.2024.54 Published online by Cambridge University Press

unknown coefficients from infinity in Equation (3) to $2N+1$ in Equation (4). The Equation (4) can be cast into the matrix form as:

$$\boldsymbol{AF} = \boldsymbol{x} \tag{5}$$

where $\boldsymbol{A}$ is a function of $\boldsymbol{W_n}$ and $\boldsymbol{\theta}$ with a dimension of m $\times$ $(2N+1)$, also known as the design matrix. The vector $\boldsymbol{F}$ contains all unknown coefficients with a dimension of $2N+1$, and $\boldsymbol{x}$ is the m-element measurement vector which contains all the measurement values at different circumferential locations. The mathematical expressions for $\boldsymbol{A}$, $\boldsymbol{F}$, and $\boldsymbol{x}$ are:

$$\boldsymbol{A} = \begin{pmatrix} \sin W_{n,1}\theta_1 & \cos W_{n,1}\theta_1 & \cdots & \sin W_{n,N}\theta_1 & \cos W_{n,N}\theta_1 & 1 \\ \sin W_{n,1}\theta_2 & \cos W_{n,1}\theta_2 & \cdots & \sin W_{n,N}\theta_2 & \cos W_{n,N}\theta_2 & 1 \\ \vdots & \vdots & \vdots & \vdots & \vdots & \vdots \\ \sin W_{n,1}\theta_m & \cos W_{n,1}\theta_m & \cdots & \sin W_{n,N}\theta_m & \cos W_{n,N}\theta_m & 1 \end{pmatrix}$$

$$\boldsymbol{F} = \begin{pmatrix} a_1 \\ b_1 \\ \vdots \\ a_N \\ b_N \\ c_0 \end{pmatrix};$$

$$\boldsymbol{x} = \begin{pmatrix} x(\theta_1) \\ x(\theta_2) \\ \vdots \\ x(\theta_m) \end{pmatrix},$$

the unknowns in $\boldsymbol{F}$ could be solved from a direct inverse matrix operation $\boldsymbol{F} = \boldsymbol{A}^{-1}\boldsymbol{x}$ when $\boldsymbol{A}$ is invertible or a least-square-fitting method for an over-determined system. To evaluate the confidence in the reconstructed signal, additional probes are required. Therefore, a minimum of $2\boldsymbol{N}+2$ measurements shall be included for resolving N wavelets of interest.

Two considerations are important while using the Fourier-based approximation method. The first is the condition number of the linear system described in Equation (6), and the second is the confidence in the reconstructed signal. The condition number of the design matrix $\boldsymbol{A}$ measures how sensitive the reconstructed signal $\boldsymbol{F}$ responds to errors in the measurements $\boldsymbol{x}$ with a smaller number indicating a 'well-conditioned' system. The condition number is calculated using the formula:

$$\boldsymbol{k} = ||\boldsymbol{A}||\,\left|\left|\boldsymbol{A}^{+}\right|\right| \tag{6}$$

where $\boldsymbol{A}^{+}$ is the inverse of matrix $\boldsymbol{A}$ for a square matrix and the Moore-Penrose pseudoinverse of matrix $\boldsymbol{A}$ for a rectangular matrix. The symbol $\|\cdot\|$ is a 2-norm used for matrix norm calculation. So, the circumferential locations $\boldsymbol{\theta}$ is chosen in a way that makes sure the condition number is small, and this can be achieved by utilising a optimisation algorithm such as particle swarm optimisation (PSO) or genetic algorithm (GA).

To evaluate the confidence in the reconstructed signal, the Pearson correlation coefficient, or Pearson's r is utilised, and it is calculated:

$$\rho = \frac{\sum_{j=1}^{m} x_j x_{fit,j} - \frac{\left(\sum_{j=1}^{m} x_j \sum_{j=1}^{m} x_{fit,j}\right)}{m}}{\sqrt{\left(\frac{\sum_{j=1}^{m} x_j^2 \left(\sum_{j=1}^{m} x_j\right)^2}{m}\right)\left(\sum_{j=1}^{m} x_{fit,j}^2 - \frac{\left(\sum_{j=1}^{m} x_{fit,j}\right)^2}{m}\right)}} \tag{7}$$

https://doi.org/10.1017/aer.2024.54 Published online by Cambridge University Press

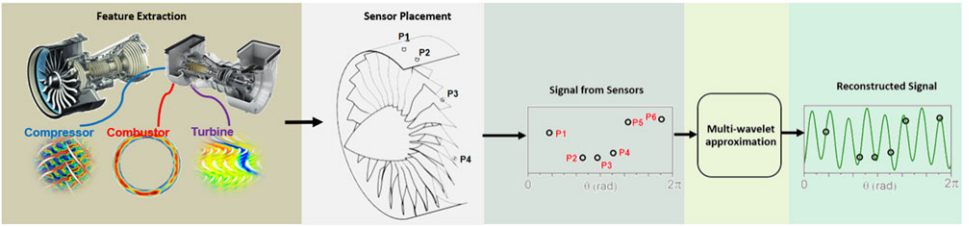

Figure 10. *Sketch of the Fourier-based approximation method.*

where $\boldsymbol{x}(\boldsymbol{\theta})$ is the true signal from measurements and $\boldsymbol{x}_{\boldsymbol{fit}}(\boldsymbol{\theta})$ represents the reconstructed signal. The range for Pearson's r is between 0 and 1. For a well-reconstructed circumferential flow field, the predicted flow properties should align with actual values at all the measurement locations and yield a value of nearly 1 for Pearson's r, and vice versa.

To summarise, the roadmap for implementation of the method is illustrated in Fig. 10 and comprises the following steps:

Pre-test:

- Identify the most significant wavenumbers/Fourier series and determine the appropriate number of probes (*refer to the empirical guidelines in Sections 1.1.1–1.1.4*).
- Employ an optimisation algorithm to select the optimal probe positions to minimise the condition number of the design matrix *A* (*refer to Section 2.1*).

Post-test:

- Reconstruct the circumferential flow using the Fourier-based approximation method (*refer to Section 2.1*).
- Assess the confidence in the reconstructed signal in terms of Pearson's r and root-mean-square of fitting residual (*refer to Section* 2.1).

2.2 Preliminary test cases

Preliminary validation of the method has been conducted using component-level rig measurements, which include total pressure measurements in a multi-stage axial compressor and total temperature measurements at the exit of a combustor and high-pressure turbine. A concise overview of each case is presented in the following session.

2.2.1 Total pressure reconstruction in a multi-stage axial compressor

First, the effectiveness of the method was evaluated using total pressure measurements obtained in a multi-stage axial compressor. The experiment took place in the Purdue 3-Stage (P3S) Axial Compressor Research Facility, utilising the PAX100 compressor with a reduced vane count for Stator 1 (referred to as PAX101). The PAX100 compressor design consists of an inlet guide vane (IGV) followed by three stages, with the vane count for each blade row listed in Table 1. A comprehensive experimental campaign was conducted to characterise the complex circumferentially nonuniform flow, following a complex vane traverse scheme developed by Kormanik [30]. Throughout the test campaign, a total of seven traverses were performed, covering approximately 58.6° of effective travel around the annulus for each rake. The implementation involved stationary rakes at three measurement locations, mapping of 19 passages for Stator 1 (S1) and 22 passages for Stator 2 (S2). These measurements allowed for a detailed assessment

https://doi.org/10.1017/aer.2024.54 Published online by Cambridge University Press

Table 1. *Number of blade/vane count for individual blade row*

Blade row index	IGV	R1	S1	R2	S2	R3	S3
Blade/Vane Count	44	36	38	33	44	30	50

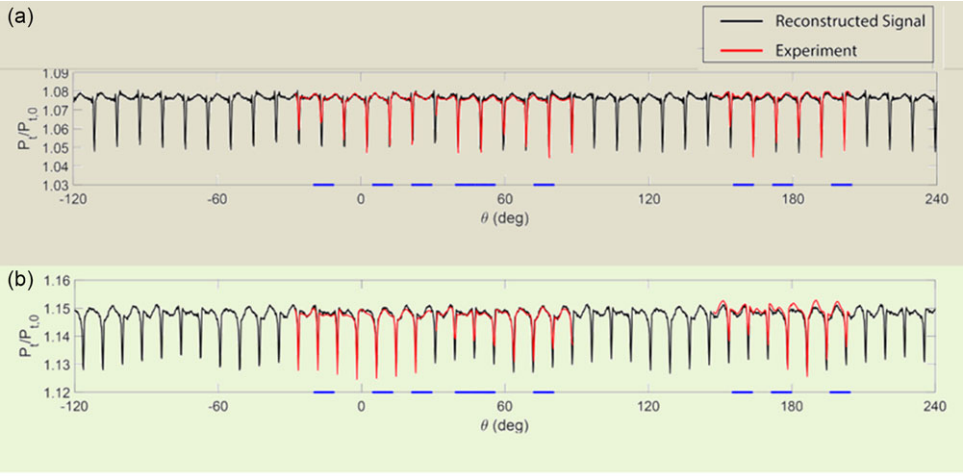

Figure 11. *Comparison of the reconstructed mid-span total pressure profiles with experiment: (a) downstream of Stator 1 and (b) downstream of Stator 2, adapted from Ref. [6].*

of the flow field's complexity and nonuniformity, which served as the foundation for validating the proposed method.

Figure 11 illustrates the reconstructed total pressure profiles downstream of S1 and S2 at midspan, employing the aforementioned Fourier-based approximation method. The figures also display results from the experiment. Blue bands on the abscissa indicate the data segments utilised for flow reconstruction, representing less than 20% of the entire annulus. Remarkably, in both cases, the reduced dataset yields impressive agreement in the total pressure profile between the reconstructed signal and the experimental data over the passages where the experimental data were used for flow reconstruction. Equally significant is the good agreement in the passages where the experimental data were not utilised for flow reconstruction. Furthermore, Fig. 12 presents the contour of the reconstructed total pressure field downstream of S1 and S2. The reconstructed total pressure profile using the reduced dataset effectively resolves features associated with passage-to-passage variations. This indicates the method's capability to accurately capture complex flow characteristics even with a reduced dataset, providing valuable insights into the flow behaviour in the multi-stage axial compressor.

Moreover, the accuracy of the mean total pressure obtained through the Fourier-based approximation method was thoroughly examined. Table 2 compares the normalised total pressure downstream of S1 and S2, derived from experimental data and the reconstructed results. Notably, the reduced dataset yields nearly identical values for the mean total pressure at all spanwise locations for both cases, with a maximum deviation of less than 0.02%.

2.2.2 Total temperature reconstruction at combustor exit

The effectiveness of the method was assessed using a whole-field combustor exit temperature profile measured at the exit plane of a typical can-annular combustor equipped with 20 fuel injectors in a military engine by QinetiQ [7], as shown in Fig. 13(a). The temperature distribution exhibited significant

https://doi.org/10.1017/aer.2024.54 Published online by Cambridge University Press

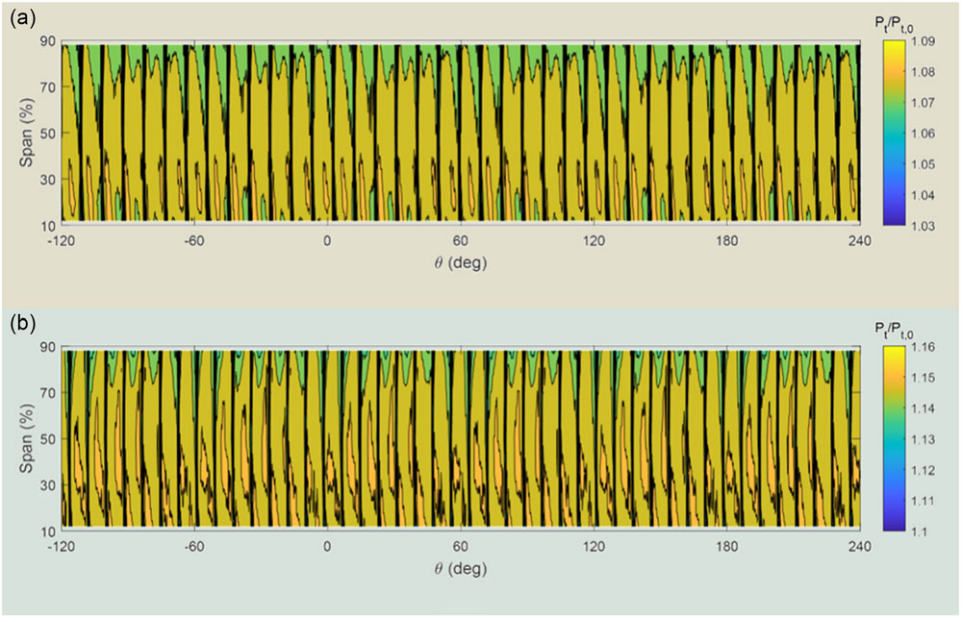

Figure 12. *Total pressure contour using the reconstructed results across the entire annulus: (a) downstream of Stator 1 and (b) downstream of Stator 2, adapted from Ref. [6].*

nonuniformities along the radial direction, with lower temperatures observed near the hub and casing regions. Additionally, prominent circumferential variations (hot-streaks) were evident, resulting from the discrete nature of the fuel injectors, and noticeable burner pitch-to-pitch variations further contributed to the temperature nonuniformities across the exit plane.

Figure 13(b) shows the reconstructed temperature profile using measurements at ten circumferential locations, employing a single-wavelet approximation method at all radii, with a wavenumber equal to the number of fuel injectors (20). The dots on the figure indicate the selected circumferential measurement locations, chosen to yield a small value of the associated condition number. The reconstructed temperature field successfully captures the primary features associated with combustor exit temperature flow. Notably, it accurately represents the temperature distributions in the cool flow regions near the hub and shroud casing end walls, as well as the hot spots in the upper-mid regions. However, the features arising from burner pitch-to-pitch asymmetry were absent in the reconstructed temperature field. Additionally, Fig. 13(c) compares the circumferentially averaged temperature radial profile obtained from the experiment and the reconstructed temperature field. The reconstructed temperature field exhibits a similar shape of the RTDF to the one obtained from the experiment. There are excellent agreements in the circumferentially averaged temperature values in the end wall regions between the reconstructed and measured flow. However, the reconstructed temperature field yields under-estimated peak circumferential averaged temperature values, with a maximum deviation of 2.4% between the reconstructed and measured results. This deviation is a consequence of the Fourier-based approximation method's limitations concerning circumferential asymmetric features and, as such, cannot be substantially reduced by increasing the number of measurements.

In summary, despite the absent burner pitch-to-pitch asymmetry information in the reconstructed temperature contour, it yields excellent agreement in the magnitude of RTDF to the experiment, with a deviation of less than half-points, listed in Table 3.

https://doi.org/10.1017/aer.2024.54 Published online by Cambridge University Press

Table 2. *Number of blade/vane count for individual blade row [5]*

	Stator 1			Stator 2		
Span (%)	Exp.	Recon	Dev (%)	Exp.	Recon	Dev (%)
12	1.0740	1.0739	0.0059	1.1465	1.1464	0.0095
20	1.0755	1.0754	0.0134	1.1473	1.1472	0.0076
35	1.0766	1.0766	0.0083	1.1482	1.1481	0.0107
50	1.0752	1.0751	0.0068	1.1471	1.1470	0.0102
70	1.0739	1.0739	0.0008	1.1459	1.1457	0.0111
80	1.0714	1.0713	0.0037	1.1438	1.1437	0.0065
88	1.0691	1.0691	0.0006	1.1409	1.1408	0.0068

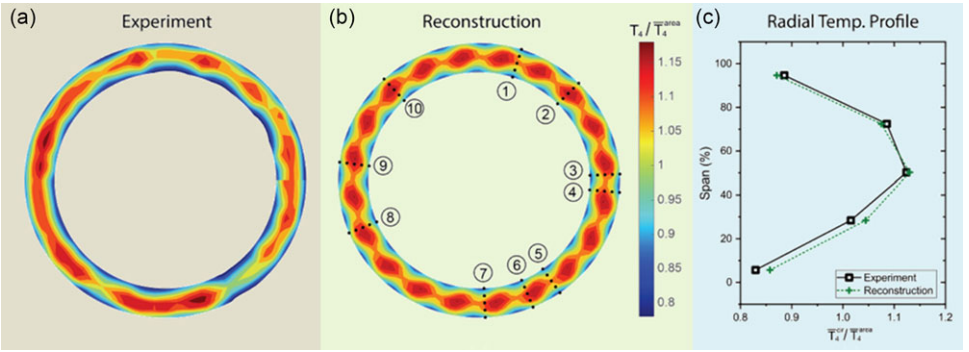

Figure 13. *Combustor exit total temperature contour using: (a) the experiment, (b) reconstructed results, and comparison of RTDF, adapted from Ref. [11].*

2.2.3 Total temperature reconstruction at HPT exit

Lastly, the Fourier-based approximation method was applied to reconstruct the total temperature at the exit of the E3 two-stage HPT. The 'true' temperature field at the HPT exit was obtained using a validated unsteady Reynolds-Averaged Navier-Stokes (URANS) solver. Two simulations were conducted to investigate the impact of burner-to-burner asymmetry on the effectiveness of the proposed method. The baseline case employed a temperature distribution with perfect burner-to-burner symmetry. In contrast, the second simulation utilised a temperature distribution with significant burner-to-burner variations to represent a more realistic condition.

Figure 14(a) illustrates the reconstructed HPT exit temperature distributions at midspan using single-, double- and triple-wavelet approximations for the baseline case. The true measurements are also included in the figure for comparison. As discussed in the previous section, multiple mechanisms drive the circumferential temperature nonuniformity at the HPT exit. As expected, employing a single-wavelet approximation results in a significant deviation in the reconstructed signal, with a 25.9% overestimation in the magnitude related to hot-streaks. However, incorporating additional wavelets leads to a substantial improvement in the reconstructed circumferential temperature distribution. Implementing a triple-wavelet approximation with wavenumbers of 18 (hot-streaks), 48 (S2 wakes) and 30 (hot-streaks and S2 interactions) achieves reasonably good agreement between the measurements and the reconstructed signal.

Figure 14(b) depicts the reconstructed HPT exit temperature distributions at midspan using single-, double- and triple-wavelet approximations for the QientiQ case. As discussed in the previous section, the presence of burner-to-burner asymmetry results in a more scattered energy distribution across the spatial

https://doi.org/10.1017/aer.2024.54 Published online by Cambridge University Press

Table 3. *Comparison of RTDF and OTDF between experimental and reconstructed results*

Par.	Experiment	Reconstruction	Error (%)
RTDF	0.138	0.135	0.3
OTDF	0.215	0.191	2.4

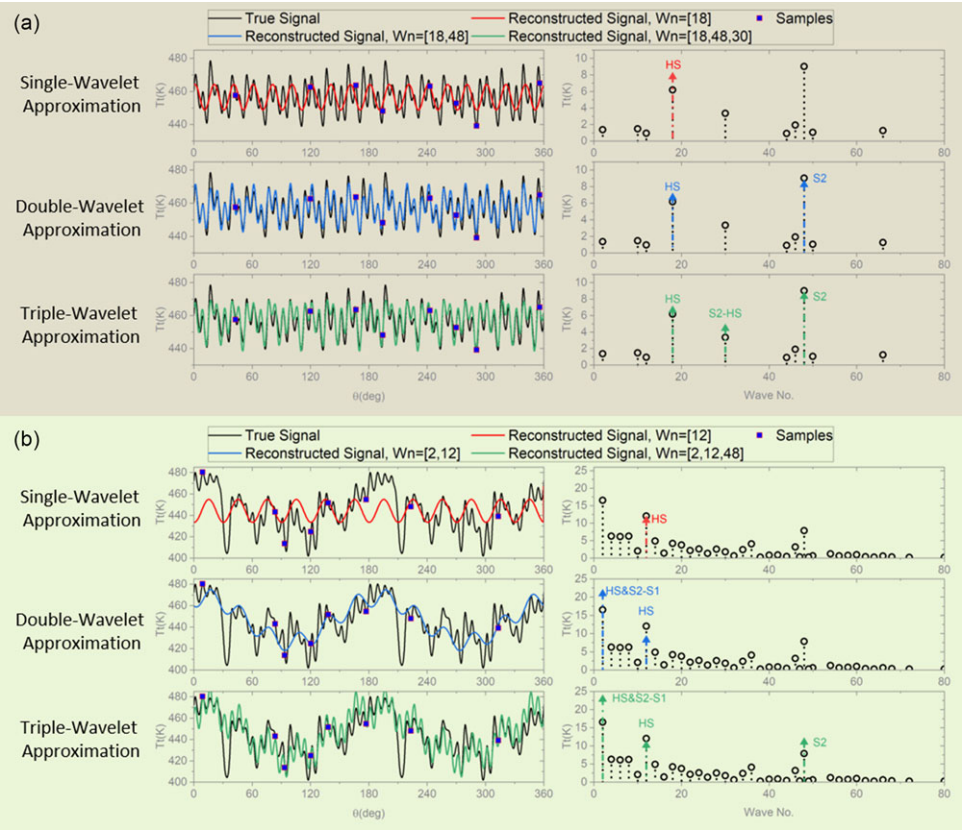

Figure 14. *Comparison of the true and predicted HPT exit total temperature profile at mid-span in spatial and frequency domain for (a) the baseline case and (b) the QinetiQ case [7], adapted from Ref. [12].*

domain, adding complexity to the situation. Nevertheless, including a second or a third wavelet significantly enhances the fidelity of the reconstructed HPT exit circumferential temperature distribution. For instance, by utilising a triple-wavelet approximation with wavenumbers of 2, 12 and 48, reasonably good agreement is achieved in both temperature distribution and hot-streaks-related magnitude between measurements and the reconstructed signal. The errors in the predicted magnitudes related to hot-streaks (Wn=12), S2 wakes (Wn=48) and the alias component (Wn=2) are -15.7%, 40.3%, and 37.9%, respectively.

In summary, the Fourier-based approximation method demonstrates remarkable robustness in resolving the temperature profile at the HPT exit with high fidelity, irrespective of the HPT inlet conditions.

https://doi.org/10.1017/aer.2024.54 Published online by Cambridge University Press

3.0 Considerations and conclusions

A few considerations have to be made by engineers prior to implementing the above-presented Fourier-based approximation method, including:

- How many measurements are required to yield an excellent reconstructed flow field and where to place them along the circumferential direction?
- How many Fourier series should be included for flow reconstruction?

It is crucial to understand the influences of these choices on the accuracy of the reconstructed signal. Considering the paper's length, detailed discussions were not included in the present paper but can be found in Refs. [11, 12, 28, and 29]. The following are a few takeaways:

- A rule of thumb is to add a minimum of two measurement counts for each Fourier serial. For a single Fourier approximation, a minimum of six locations is required to yield a reconstructed signal with good fidelity. The benefit of increasing the measurement count depends on the number of dominant Fourier series and is case-dependent.
- The condition number of the design matrix plays an important role in the quality of the reconstructed signal. Thus, an intelligent selection of the probe positions must be exercised. An optimal set of probe positions yields a smaller condition number for the design matrix. A rule of thumb is that a condition number less than 2.0 shall be targeted when using a single Fourier serial for flow reconstruction.

To conclude, th4 following are a few underlying fundamentals for resolving the nonuniform flow in gas turbines:

- Flow in gas turbine engines is fundamentally unsteady and non-uniform. In other words, nonuniformity is everywhere in gas turbines, it introduces instrumentation errors, contributing to uncertainties when calculating one-dimensional performance metrics during rig or engine tests using fixed-location rakes. Additionally, it raises mechanical concerns, including high cycle fatigue due to blade row interactions in turbomachines and thermal fatigue caused by hot-streaks at the combustor exit.
- The circumferential flow nonuniformity (especially the temperature and pressure field) in gas turbines is typically dominated by a few flow features and commonly periodic along the annulus; in other words, it is a sparse function in the spatial-frequency domain. This conclusion has been widely supported by previous research.
- Therefore, it is possible to approximate the circumferential nonuniformity in terms of a limited number of Fourier series with reasonably well accuracy.
- The Fourier-based approximation method shows good potential in characterising the inter-stage circumferential pressure nonuniformity and temperature nonuniformity at the combustor or HPT exit.
- A few considerations must be taken, including an intelligent selection of probe count and positions, dominant wavenumbers, etc., prior to implementing the proposed Fourier-based approximation method.

4.0 Moving forward

While the proposed methodology shows promising outcomes, continued research is necessary to enhance its fidelity and expand its applicability. To this end, the author recommends exploring two key topics for future investigations.

https://doi.org/10.1017/aer.2024.54 Published online by Cambridge University Press

Modelling of asymmetric flow phenomena: An important limitation of the 'Fourier-based approximation method' is its inability to resolve circumferential asymmetric features accurately. For instance, in the QinetiQ case [7], the method yields a 2.4% deviation in the predicted peak circumferential averaged temperature at the combustor exit due to evident burner pitch-to-pitch variability. Besides burner pitch-to-pitch asymmetry, other factors can contribute to circumferential asymmetry, such as inlet distortion, bleed, casing eccentricity, etc. Unfortunately, increasing the number of measurements does not alleviate this shortcoming in the Fourier-based approximation method. Thus, it is crucial to develop models to account for asymmetry flow phenomena in gas turbines.

Data fusion with multi-fidelity results: The Fourier-based approximation method is fundamentally a model-based technique, with its tuning relying on experimental data. While it effectively captures dominant flow features, it may not preserve all flow characteristics. Hence, exploring data fusion with multi-fidelity results, such as high-fidelity experimental measurements, medium-fidelity model-driven predictions, and low-fidelity numerical simulations, holds significant potential. The method can be enriched by incorporating information from different sources, enhancing its accuracy and encompassing a broader range of flow features.

Acknowledgments. The authors would like to acknowledge the support from National Science and Technology Major Project (J2019-I-0007-0007).

References

[1] Sadrehaghighi, I. An example reference, 2023. doi: 10.13140/RG.2.2.13712.12801/4, p 95.
[2] Migliorini, M., Zachos, P.K., MacManus, D.G. and Haladuda, P. S-duct flow distortion with non-uniform inlet conditions, *Proc. Inst. Mech. Eng. Part G J. Aerospace Eng.*, 2023, **237,** (2), pp 357–373.
[3] Sheoran, Y., Bouldin, B. and Krishnan, P.M. Compressor performance and operability in swirl distortion, in *Turbo Expo: Power for Land, Sea, and Air*, vol. **44021**, 2010, pp 2453–2464.
[4] Chilla, M., Pullan, G. and Gallimore, S. Reducing instrumentation errors caused by circumferential flow-field variations in multistage axial compressors, *J. Turbomach.*, 2020, **142,** (9), p 091006.
[5] Kormanik, N.J., Matthews, D.R., Key, N.L. and King, A.J. Purdue 3-stage axial compressor research facility: Through the years, to infinity, and beyond, AIAA Propulsion and Energy 2019 Forum, 2019, p 4000.
[6] Lou, F., Matthews, D.R., Kormanik III, N.J. and Key, N.L. Accounting for circumferential flow nonuniformity in a multistage axial compressor, *J. Turbomach.*, 2023, **145,** (7), p 071016.
[7] Povey, T., Chana, K.S., Jones, T.V. and Hurrion, J. The effect of hot-streaks on HP vane surface and endwall heat transfer: An experimental and numerical study, *J. Turbomach.*, 2007, **129,** (1), pp 32–43.
[8] Povey, T. and Qureshi, I. Developments in hot-streak simulators for turbine testing, *J. Turbomach.*, 2009, **131,** (3), p 031009.
[9] Goebel, S.G., Abuaf, N., Lovett, J.A. and Lee, C.P. Measurements of combustor velocity and turbulence profiles, Turbo Expo: Power for Land, Sea, and Air, vol. 78903, American Society of Mechanical Engineers, 1993, p V03AT15A079.
[10] Barringer, M.D., Thole, K.A. and Polanka, M.D. Experimental evaluation of an inlet profile generator for high-pressure turbine tests. *J. Turbomach.*, 2007, **129,** (2), pp 382–393.
[11] Lou, F. Approximating gas turbine combustor exit temperature distribution factors using spatially under-sampled measurements, *J. Eng. Gas Turbines Power*, 2022, **144,** (10), p 101018.
[12] Zhu, X., Zhou, K., Zheng, X. and Lou, F. Lessons learned toward estimating the high-pressure turbine inlet temperature profile using measurements acquired at the high-pressure turbine exit, *J. Eng. Gas Turbines Power*, 2023, **145,** (7).
[13] Adamczuk, R.R. and Seume, J.R. Time resolved full-annulus computations of a turbine with inhomogeneous inlet conditions, *Int. J. Gas Turbine Propul. Power Syst.*, 2012, **4,** (2), pp 1–7.
[14] Chi, Z., Liu, H., Zang, S., Pan, C. and Zhang, M. Full-annulus URANS study of inlet hot-streak transportation in a four-stage gas turbine, Turbo Expo: Power for Land, Sea, and Air, vol. 50992, American Society of Mechanical Engineers, 2018, p V02AT45A011.
[15] Stoll, F., Tremback, J.W. and Arnaiz, H.H. *Effect of number of probes and their orientation on the calculation of several compressor face distortion descriptors* (No. NASA-TM-72859), 1979.
[16] Cumpsty, N. and Horlock, J.H. Averaging nonuniform flow for a purpose, *J. Turbomach.*, 2006, **128,** (1), pp 120–129.
[17] He, L., Chen, T., Wells, R.G., Li, Y.S. and Ning, W. Analysis of rotor-rotor and stator-stator interferences in multi-stage turbomachines, Turbo Expo: Power for Land, Sea, and Air, vol. 3610, 2002, pp 287–298.
[18] Methel, J., Smith, N.R., Berdanier, R.A. and Key, N.L. Effects of circumferential nonuniformity in compressor flow fields including vane wake variability, *J. Propul. Power*, 2018, **34,** (4), pp 1080–1089.
[19] Besem, F.M., Kielb, R.E., Galpin, P., Zori, L. and Key, N.L. Mistuned forced response predictions of an embedded rotor in a multistage compressor, *J. Turbomach.*, 2016, **138,** (6), p 061003.
[20] Li, J., Aye-Addo, N., Kielb, R. and Key, N. Mistuned higher-order mode forced response of an embedded compressor rotor—part II: Mistuned forced response prediction, *J. Turbomach.*, 2018, **140,** (3), p 031006.

[21] Schoenenborn, H. Analysis of the effect of multirow and multipassage aerodynamic interaction on the forced response variation in a compressor configuration—Part I: Aerodynamic excitation, *J. Turbomach.*, 2018, **140,** (5), p 051004.
[22] Chilla, M., Pullan, G. and Thorne, G. Sensitivity of multi-stage compressor performance assessment to measurement rake positions, Turbo Expo: Power for Land, Sea, and Air, vol. 84065, American Society of Mechanical Engineers, 2020, p V02AT32A019.
[23] Seshadri, P., Simpson, D., Thorne, G., Duncan, A. and Parks, G. Spatial flow-field approximation using few thermodynamic measurements—Part I: Formulation and area averaging, *J. Turbomach.*, 2020, **142,** (2), p 021006.
[24] Seshadri, P., Duncan, A., Simpson, D., Thorne, G. and Parks, G. Spatial flow-field approximation using few thermodynamic measurements—Part II: Uncertainty assessments. *J. Turbomach.*, 2020, **142,** (2), p 021007.
[25] Seshadri, P., Duncan, A.B., Thorne, G., Parks, G., Diaz, R.V. and Girolami, M. Bayesian assessments of aeroengine performance with transfer learning, *Data-Centric Eng.*, 2022, **3**, e29.
[26] Cruz, G.G., Babin, C., Ottavy, X. and Fontaneto, F. Bayesian inference of experimental data for axial compressor performance assessment, Turbo Expo: Power for Land, Sea, and Air, vol. 84904, American Society of Mechanical Engineers, 2021, p. V02AT31A029.
[27] Cruz, G.G., Babin, C., Ottavy, X. and Fontaneto, F. A Bayesian data driven multi-fidelity modelling approach for experimental under-sampled flow reconstruction, Turbo Expo: Power for Land, Sea, and Air, American Society of Mechanical Engineers, 2023.
[28] Lou, F. and Key, N.L. Reconstructing compressor non-uniform circumferential flow field from spatially undersampled data—Part 1: Methodology and sensitivity analysis, *J. Turbomach.*, 2021, **143,** (8), p 081002.
[29] Lou, F., Matthews, D.R., Kormanik, N.J.K. and Key, N.L. Reconstructing compressor nonuniform circumferential flow field from spatially undersampled data – Part 2: Practical application for experiments, *J. Turbomach.*, 2021, **143,** (8), p 081003.
[30] Kormanik III, N.J. Characterization of aerodynamic forcing functions for embedded rotor resonant response in a multistage compressor, MS thesis, Mechanical Engineering, Purdue University, West Lafayette, IN, 2017.

Cite this article: Lou F. (2024). Resolving nonuniform flow in gas turbines: challenges, progress, and moving forward. *The Aeronautical Journal*, **128**, 1325–1343. https://doi.org/10.1017/aer.2024.54